

Effect of initial phase on the Rayleigh-Taylor instability of a finite-thickness fluid shell

Hong-Yu Guo(郭宏宇), Tao Cheng(程涛), Jing Li(李景), and Ying-Jun Li(李英骏)
Citation: Chin. Phys. B, 2022, 31 (**3**): 035203. DOI: 10.1088/1674-1056/ac3390
Journal homepage: http://cpb.iphy.ac.cn; http://iopscience.iop.org/cpb

What follows is a list of articles you may be interested in

Scaling of rise time of drive current on development of magneto-Rayleigh-Taylor instabilities for single-shell Z-pinches

Xiaoguang Wang(王小光), Guanqiong Wang(王冠琼), Shunkai Sun(孙顺凯), Delong Xiao(肖德龙), Ning Ding(丁宁), Chongyang Mao(毛重阳), and Xiaojian Shu(束小建)
Chin. Phys. B, 2022, 31 (**2**): 025203. DOI: 10.1088/1674-1056/ac1fd9

Weakly nonlinear multi-mode Bell–Plesset growth in cylindrical geometry

Hong-Yu Guo(郭宏宇), Tao Cheng(程涛), and Ying-Jun Li(李英骏)
Chin. Phys. B, 2020, 29 (**11**): 115202. DOI: 10.1088/1674-1056/ab9c14

Numerical study on magneto-Rayleigh-Taylor instabilities for thin liner implosions on the primary test stand facility

Xiao-Guang Wang(王小光), Shun-Kai Sun(孙顺凯), De-Long Xiao(肖德龙), Guan-Qiong Wang(王冠琼), Yang Zhang(张扬), Shao-Tong Zhou(周少彤), Xiao-Dong Ren(任晓东), Qiang Xu(徐强), Xian-Bin Huang(黄显宾), Ning Ding(丁宁), Xiao-Jian Shu(束小建)
Chin. Phys. B, 2019, 28 (**3**): 035201. DOI: 10.1088/1674-1056/28/3/035201

Coupling between velocity and interface perturbations in cylindrical Rayleigh-Taylor instability

Hong-Yu Guo(郭宏宇), Li-Feng Wang(王立锋), Wen-Hua Ye(叶文华), Jun-Feng Wu(吴俊峰), Wei-Yan Zhang(张维岩)
Chin. Phys. B, 2018, 27 (**5**): 055205. DOI: 10.1088/1674-1056/27/5/055205

Rayleigh-Taylor instability at spherical interfaces of incompressible fluids

Hong-Yu Guo(郭宏宇), Li-Feng Wang(王立锋), Wen-Hua Ye(叶文华), Jun-Feng Wu(吴俊峰), Ying-Jun Li(李英骏), Wei-Yan Zhang(张维岩)
Chin. Phys. B, 2018, 27 (**2**): 025206. DOI: 10.1088/1674-1056/27/2/025206

Effect of initial phase on the Rayleigh–Taylor instability of a finite-thickness fluid shell

Hong-Yu Guo(郭宏宇)[1,2,†], Tao Cheng(程涛)[1,2], Jing Li(李景)[3], and Ying-Jun Li(李英骏)[1,2,‡]

[1] *State Key Laboratory for Geomechanics and Deep Underground Engineering, China University of Mining and Technology, Beijing* 100083, *China*
[2] *School of Science, China University of Mining and Technology, Beijing* 100083, *China*
[3] *Beijing Aeronautical Technology Research Center, Beijing* 100076, *China*

(Received 29 July 2021; revised manuscript received 4 October 2021; accepted manuscript online 27 October 2021)

Rayleigh–Taylor instability (RTI) of finite-thickness shell plays an important role in deep understanding the characteristics of shell deformation and material mixing. The RTI of a finite-thickness fluid layer is studied analytically considering an arbitrary perturbation phase difference on the two interfaces of the shell. The third-order weakly nonlinear (WN) solutions for RTI are derived. It is found the main feature (bubble-spike structure) of the interface is not affected by phase difference. However, the positions of bubble and spike are sensitive to the initial phase difference, especially for a thin shell ($kd < 1$), which will be detrimental to the integrity of the shell. Furthermore, the larger phase difference results in much more serious RTI growth, significant shell deformation can be obtained in the WN stage for perturbations with large phase difference. Therefore, it should be considered in applications where the interface coupling and perturbation phase effects are important, such as inertial confinement fusion.

Keywords: Rayleigh–Taylor instability, interface coupling effect, inertial confinement fusion

PACS: 52.57.Fg, 47.20.Ma, 52.35.Py **DOI:** 10.1088/1674-1056/ac3390

1. Introduction

When the heavier fluid is supported or accelerated by the lighter one, the perturbed fluid interface between two fluids is subject to Rayleigh–Taylor instability (RTI).[1,2] RTI is widely exist in laboratory experiments, such as magneto-inertial fusion (MIF)[3] and inertial confinement fusion (ICF).[4,5] The RTI is considered to be a critical mechanism for the whole perturbation growth in ICF implosions.[4] The typical ICF central ignition capsule contains two fluid layers, the imploded fuel shell is distributed on the inside and the outside is surrounded by an ablation layer. Therefore, there are at least three interfaces for the implosion capsule, namely, the ablation interface, the fuel–ablator interface, and the hot-spot interface. During the acceleration phase of the implosion, the high density fuel shell is accelerated by the ablative plasma and the ablation interface is subject to RTI. The hot-spot interface is also suffer to RTI in the deceleration stage where the heavy fuel shell is decelerated by the internal light hot-spot. The RTI growth can cause the ablator material to mix into the hot-spot, limit the implosion compression of the fuel, and even destroy the integrity of the implosion shell. More seriously, the RTI would hinder the formation of hot-spots, resulting in the degradation of ICF implosions. Because of its importance and significance to the basic research and engineering application for ICF implosion, it is still a key issue to investigate the RTI growth in the ICF implosions.

The classical RTI (CRTI) is first studied analytically by Rayleigh[1] and Taylor,[2] the linear growth for two semi-infinity fluids is derived. It is found that small perturbations at the fluid interface grow exponentially in time, *i.e.*, $\eta(t)/\eta_0 \sim e^{\gamma t}$, where $\gamma = \sqrt{Akg}$ is growth rate and η_0 is the initial perturbation amplitude, A is the Atwood number at the interface, k is perturbation wave-number, and g is the gravitational acceleration. Most researchers deal with classical RTI model of two semi-infinity fluids with a single-interface.[6–11] However, we want to investigate an accelerated thin shell in ICF implosion. How perturbations on one interface are transmitted to another interface is a critical issue for ICF implosion. Mikaelian[12,13] studied the linear growth of RTI for arbitrary number of stratified fluids, the linear growth rate and the interface coupling effect is discussed analytically. Recently, we have investigated the linear growth of RTI in planar,[14] cylindrical,[15] and spherical geometry,[16] the explicit interface coupling phenomenons are analyzed. Weis[17] studied the RTI growth on a finite plasma slab with an arbitrary magnitude magnetic field and obtained the feedthrough factor between the slab interfaces. The RTI of finite-thickness shell in spherical and cylindrical geometry are discussed by Velikovich[18] with Bell–Plesset effects[19] into consideration. All these works mentioned above are about linear growth of RTI, the experiment results[20,21] have confirmed that the perturbation is in the linear stage when the perturbation amplitude $\eta(t)$ is less than the wavelength λ ($\eta(t) \ll \lambda$). When the perturbation ampli-

†Corresponding author. E-mail: ghy@cumtb.edu.cn
‡Corresponding author. E-mail: lyj@aphy.iphy.ac.cn

© 2022 Chinese Physical Society and IOP Publishing Ltd

tude grows to be comparable to the perturbation wavelength, $k\eta(t) \sim 1$, the perturbation begins to enter into the weakly nonlinear (WN) stage. The initially symmetrical interface will transform into an irregular bubble-spike-like structure. The WN model can be used to describe the RTI growth and the interface deformation in WN stage, which is consistent with the experiment results.[21,22] Jacobs[6] developed a third-order WN model of $A = 1$ to study three-dimensional CRTI with different interface symmetries (rectangular, circular, and hexagonal). The CRTI for arbitrary Atwood number A with initial interface and velocity perturbations are studied by Wang.[8] It is found the coupled interface and velocity perturbations play an important role in the experiment.[20] Recently, a single-mode WN model for RTI growth on finite-thickness fluid shell is established,[23,24] the perturbation growth and the shell deformation is illustrated clearly. All these works are about perturbations at the shell interfaces with the same phase. Due to the inhomogeneity of the imploded shell and the asymmetry of the laser drive, the phases of the perturbations at the interfaces are random. The evolution of interface instability is affected by small-scale details of the initial phase condition until later nonlinear stage.[25] In this research, the RTI growth for finite-thickness shell in WN stage is presented where the perturbations on the shell interfaces are initiated with an arbitrary phase difference.

2. Theoretical model

In the present work, a finite-thickness shell with fluid density ρ and thickness d is immersed in a gravitational field $-g\hat{e}_y$, as displayed in Fig. 1. Both sides of the fluid shell are vacuum. The finite-thickness fluid is considered to be incompressible, irrotational, inviscid, and immiscible. A two-dimensional Cartesian coordinate is used, where x and y are along and normal to the upper interface of the fluid shell, respectively. The unperturbed upper and lower interfaces are located at $y = 0$ and $-d$, respectively. In the following discussion, the physical quantities on the upper interface are indicated by superscript "u" and that on the lower interface by "l", unless otherwise indicated.

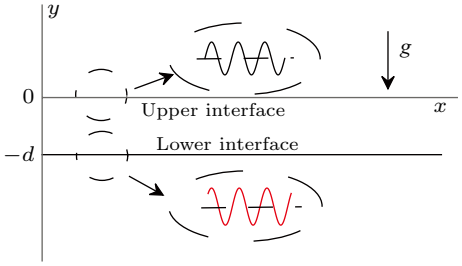


Fig. 1. Schematic drawing of finite-thickness fluid shell considered in this paper.

The velocity potential related to the incompressible fluid that can be written as

$$\phi(x,y,t) = \phi_{(0)}(t) + \varphi(x,y,t), \tag{1}$$

where $\phi_{(0)}(t)$ is unperturbed velocity potential and $\varphi(x,y,t)$ is the perturbed velocity potential. The Bernoulli equations which describe the pressure conditions at the upper and lower interfaces are

$$p^{\mathrm{u}}_{(0)} + \tilde{p}^{\mathrm{u}} = -\rho\left[\phi_t + \frac{1}{2}(\nabla\phi)^2 + g\eta^{\mathrm{u}} + f(t)\right], \tag{2}$$

$$p^{\mathrm{l}}_{(0)} + \tilde{p}^{\mathrm{l}} = -\rho\left[\phi_t + \frac{1}{2}(\nabla\phi)^2 + g\eta^{\mathrm{l}} - gd + f(t)\right], \tag{3}$$

where $p^{\mathrm{u}}_{(0)}$ and $p^{\mathrm{l}}_{(0)}$ are the unperturbed pressures at the two interfaces. Thus, the unperturbed pressures at the upper and lower interfaces are

$$p^{\mathrm{u}}_{(0)} = -\rho\left[\dot{\phi}_{(0)}(t) + f(t)\right], \tag{4}$$

$$p^{\mathrm{l}}_{(0)} = -\rho\left[\dot{\phi}_{(0)}(t) - gd + f(t)\right], \tag{5}$$

where the dot above represents the derivative of time. As can be seen, the equilibrium pressure condition $p^{\mathrm{l}}_{(0)} - p^{\mathrm{u}}_{(0)} = \rho gd$ has been satisfied. Therefore, the perturbed pressures can be obtained as

$$\tilde{p}^i = -\rho\left[\varphi_t + \frac{1}{2}\left(\varphi_x^2 + \varphi_y^2\right) + g\eta^i\right], \tag{6}$$

where $i = \mathrm{u},\mathrm{l}$ represents the physical quantities at the upper and lower interfaces. For a finite-thickness fluid layer in a gravitational field, the perturbed pressures at the two interfaces are zero,[23,24] namely, $\tilde{p}^i = 0$. The kinematic conditions at the upper and lower interfaces are

$$\eta^i_t + \varphi_x \cdot \eta^i_x - \varphi_y = 0, \tag{7}$$

which means the normal components of velocity at the two interfaces are continuous.

Considering the initially single-mode perturbations at the upper and lower interfaces have an arbitrary phase difference. Then, the perturbations and perturbed velocity potential are expressed in the first-order as

$$\eta^{\mathrm{u}}_{(1)}(x,t) = u^{\mathrm{c}}_1(t)\cos(kx) + u^{\mathrm{s}}_1(t)\sin(kx), \tag{8}$$

$$\eta^{\mathrm{l}}_{(1)}(x,t) = l^{\mathrm{c}}_1(t)\cos(kx) + l^{\mathrm{s}}_1(t)\sin(kx), \tag{9}$$

$$\begin{aligned}\varphi_{(1)}(x,y,t) = {} & \left[a_1(t)\mathrm{e}^{ky} + b_1(t)\mathrm{e}^{-ky}\right]\cos(kx) \\ & + \left[c_1(t)\mathrm{e}^{ky} + d_1(t)\mathrm{e}^{-ky}\right]\sin(kx),\end{aligned} \tag{10}$$

Substituting Eqs. (8)–(10) into Eqs. (6) and (7), the governing equations for $u^{\mathrm{c}}_1(t)$, $u^{\mathrm{s}}_1(t)$, $l^{\mathrm{c}}_1(t)$, and $l^{\mathrm{s}}_1(t)$ are obtained. Considering there are single-mode cosinusoidal perturbations at the upper and lower interfaces with an arbitrary phase defference, which can be expressed as

$$\eta^{\mathrm{u}}_{(1)}(x,t=0) = A_0\cos(kx+\theta), \tag{11}$$

$$\eta^{\mathrm{l}}_{(1)}(x,t=0) = B_0\cos(kx), \tag{12}$$

where A_0 and B_0 are initial perturbation amplitudes at the upper and lower interfaces, θ is the initial phase difference of the perturbations at the two interfaces. Then, using the initial conditions Eqs. (11) and (12), the linear solutions for the RTI growth of the perturbations are derived as

$$\begin{aligned}\eta^{\rm u}_{(1)} &= {\rm e}^{-\xi}\Big[(\Xi_A\cos\theta+\Xi_B)\cosh(\gamma t)\\ &\quad-\Big(\Xi_A\cos\theta{\rm e}^{2\xi}+\Xi_B\Big)\cos(\gamma t)\Big]\cos(kx)\\ &\quad+\Xi_A\sin\theta\Big[{\rm e}^{\xi}\cos(\gamma t)-{\rm e}^{-\xi}\cosh(\gamma t)\Big]\sin(kx), \quad (13)\\ \eta^{\rm l}_{(1)} &= \Big[(\Xi_A\cos\theta+\Xi_B)\cosh(\gamma t)\\ &\quad-\Big(\Xi_A\cos\theta+\Xi_B{\rm e}^{-2\xi}\Big)\cos(\gamma t)\Big]\cos(kx)\\ &\quad+\Xi_A\sin\theta[\cos(\gamma t)-\cosh(\gamma t)]\sin(kx), \quad (14)\end{aligned}$$

where $\gamma=\sqrt{kg}$ is the growth rate and $\xi=kd$ is the normalized fluid thickness. The coefficients $\Xi_A=-A_0{\rm e}^{-\xi}/(1-{\rm e}^{-2\xi})$ and $\Xi_B=B_0/(1-{\rm e}^{-2\xi})$. As can be seen, perturbations on the two interfaces are coupled especially for a thin shell ($\xi<1$), the coupling effect is represented by Ξ_A, Ξ_B, and ${\rm e}^{-\xi}$. The linear growth rate γ is independent on the phase difference θ. However, interface deformation and the perturbation amplitudes are affected by θ, which will be discussed later. When the perturbations at the two interfaces are in phase ($\theta=0$), the linear results of CRTI in Refs. [2,24] are recovered.

In order to investigate the weakly nonlinear (WN) growth of the finite-thickness RTI with an arbitrary phase difference into consideration, the oscillation terms (*i.e.*, $\cos(\gamma t)$) and the terms decaying exponentially in time (*i.e.*, ${\rm e}^{-\gamma t}$) are dropped, keeping only the dominate terms (*i.e.*, ${\rm e}^{\gamma t}$, ${\rm e}^{2\gamma t}$, ${\rm e}^{3\gamma t}$) at each order.[23,24] Thus, at arbitrary time t, the interface perturbations $\eta^{\rm u}(x,t)$, $\eta^{\rm l}(x,t)$, and velocity potential $\varphi(x,y,t)$ can be expanded into the third-order in a formal parameter ε as

$$\begin{aligned}\eta^{\rm u}_{(3)}(x,t) &= \sum_{n=1}^{3}\varepsilon^n\Big[u_n^{\cos}(t)\cos(nkx)+u_n^{\sin}(t)\sin(nkx)\Big], \quad (15)\\ \eta^{\rm l}_{(3)}(x,t) &= \sum_{n=1}^{3}\varepsilon^n\Big[l_n^{\cos}(t)\cos(nkx)+l_n^{\sin}(t)\sin(nkx)\Big], \quad (16)\\ \varphi(x,y,t) &= \sum_{n=1}^{3}\varepsilon^n\Big[\varphi_n^{\cos}(y,t)\cos(nkx)\\ &\quad+\varphi_n^{\sin}(y,t)\sin(nkx)\Big], \quad (17)\end{aligned}$$

the perturbation amplitudes are $u_n^{\cos}(t)=\sum_{j=0}^{N}u^{\rm c}_{m,n}{\rm e}^{n\gamma t}$ and $u_n^{\sin}(t)=\sum_{j=0}^{N}u^{\rm s}_{m,n}{\rm e}^{n\gamma t}$, where $m=n+2j$ and $N=\lfloor(3-n)/2\rfloor$ is Gauss's symbol which represents the maximum integer less than or equal to $(3-n)/2$. The corresponding perturbation amplitudes at the lower interface are $l_n^{\cos}(t)=\sum_{j=0}^{N}l^{\rm c}_{m,n}{\rm e}^{n\gamma t}$ and $l_n^{\sin}(t)=\sum_{j=0}^{N}l^{\rm s}_{m,n}{\rm e}^{n\gamma t}$. The amplitudes for velocity potentials are $\varphi_n^{\cos}=\sum_{j=0}^{N}\left(a_{m,n}{\rm e}^{ky}+b_{m,n}{\rm e}^{-ky}\right){\rm e}^{n\gamma t}$ and $\varphi_n^{\sin}=\sum_{j=0}^{N}\left(c_{m,n}{\rm e}^{ky}+d_{m,n}{\rm e}^{-ky}\right){\rm e}^{n\gamma t}$. The perturbed velocity potential already satisfies the Laplace equation $\nabla^2\varphi=0$. The $u^{\rm c}_{m,n}$ ($u^{\rm s}_{m,n}$) are the amplitudes of n-th cosinusoidal (sinusoidal) Fourier harmonic in the m-th order of ε on the upper interface. The $l^{\rm c}_{m,n}$ ($l^{\rm s}_{m,n}$) are the corresponding amplitudes on the lower interface. The amplitudes $u^{\rm c}_{m,n}$, $u^{\rm s}_{m,n}$, $l^{\rm c}_{m,n}$, and $l^{\rm s}_{m,n}$ depend on shell thickness d and initial phase difference θ which are unknowns that we want to obtain. Substituting Eqs. (15)–(17) into Eqs. (6) and (7), picking out terms with the same power of parameter ε^n to establish the governing equation. Then, we can solve these resulting equations step by step for $n=1,2,3$. The amplitudes of first three cosine harmonics at the lower interface are derived as

$$l^{\rm c}_{1,1}=\Xi_A\cos\theta+\Xi_B, \quad (18)$$

$$l^{\rm c}_{2,2}=-\frac{1}{2}k\left(\Xi_A^2\cos(2\theta)+2\cos\theta\Xi_A\Xi_B+\Xi_B^2\right), \quad (19)$$

$$\begin{aligned}l^{\rm c}_{3,3} &= \frac{3}{8}k^2l^{\rm c}_{1,1}\big[(2\cos(2\theta)-1)\Xi_A^2\\ &\quad+2\cos\theta\Xi_A\Xi_B+\Xi_B^2\big], \quad (20)\end{aligned}$$

$$\begin{aligned}l^{\rm c}_{3,1} &= -\frac{1}{8}k^2l^{\rm c}_{1,1}\left(3{\rm e}^{-2\xi}+2\right)\\ &\quad\times\left(\Xi_A^2+2\cos\theta\Xi_A\Xi_B+\Xi_B^2\right). \quad (21)\end{aligned}$$

The corresponding amplitudes for sine harmonics are obtained simultaneously as

$$l^{\rm s}_{1,1}=-\Xi_A\sin\theta, \quad (22)$$

$$l^{\rm s}_{2,2}=-kl^{\rm s}_{1,1}l^{\rm c}_{1,1}, \quad (23)$$

$$\begin{aligned}l^{\rm s}_{3,3} &= \frac{3}{8}k^2l^{\rm s}_{1,1}\big[(2\cos(2\theta)+1)\Xi_A^2\\ &\quad+6\cos\theta\Xi_A\Xi_B+3\Xi_B^2\big], \quad (24)\end{aligned}$$

$$\begin{aligned}l^{\rm s}_{3,1} &= -\frac{1}{8}k^2l^{\rm s}_{1,1}\left(3{\rm e}^{-2\xi}+2\right)\\ &\quad\times\left(\Xi_A^2+2\cos\theta\Xi_A\Xi_B+\Xi_B^2\right). \quad (25)\end{aligned}$$

The perturbation amplitudes $u^{\rm c}_{m,n}$ and $u^{\rm s}_{m,n}$ at the upper interfaces are

$$u^{\rm c(s)}_{m,n}=\begin{cases}l^{\rm c(s)}_{m,n}{\rm e}^{-n\xi}, & m=n,\\ l^{\rm c(s)}_{m,n}{\rm e}^{-\xi}\dfrac{\left(3+2{\rm e}^{-2\xi}\right)}{\left(2+3{\rm e}^{-2\xi}\right)}, & m\neq n.\end{cases} \quad (26)$$

If the initial phase difference $\theta=0$, the classical third-order WN results for finite-thickness RTI are recovered.[23,24] As can be seen, the perturbation growth and interface deformation of finite-thickness are dependent on the shell thickness and the initial phase difference θ. That means phase difference θ plays an important role in WN evolution of finite RTI which will be discussed in the following.

3. Results and discussion

In this section, the WN evolutions of RTI on the two interfaces of finite-thickness shell with arbitrary phase difference θ are studied. The dependence of interface deformation and bubble-spike growth on the shell thickness and phase difference are illustrated in some detail.

In Fig. 2, temporal evolutions of perturbed upper and lower interfaces are displayed at $\gamma t = 5.0$ for initial phase difference $\theta = 0, \pi/4, 3\pi/5$, and π. The initial perturbation amplitudes are $A_0 = B_0 = 0.001\lambda$, where $\lambda = 2\pi/k$ is the perturbation wavelength with $k = 1$. The $\theta = 0$ (in phase) case for finite-thickness RTI[24] is shown for comparison. As can be seen, initial cosinusoidal perturbations develop into bubble-spike structure in the WN stage for a thin shell. Because of the interface coupling effect, the upper interface (initially stable) also becomes unstable. The larger phase difference θ leads to more obviously irregular deformation of the shell. Although the initial phases of perturbations on the upper and lower interfaces are different, the phases of the perturbation growth at the two interfaces become the same with time proceeding. That means only a bubble and a spike exist in one period along the horizontal direction. However, we can also found that the positions of the bubble and the spike are related to the initial phase difference θ. When the perturbations on two interfaces are in phase ($\theta = 0$), the spike position is $x_{\rm spike} = 0.5\lambda$. When phase difference is $\theta = \pi/4$, the position of spike is $x_{\rm spike} \sim 0.618\lambda$. In ICF implosions, the perturbation source at the interfaces of the shell can be either initial perturbations or feedthrough among the shell during the implosion. As the perturbations on the two interfaces are random, perturbations on the two interfaces with phase difference will be a common phenomenon in the process of ICF implosion that should be considered carefully.

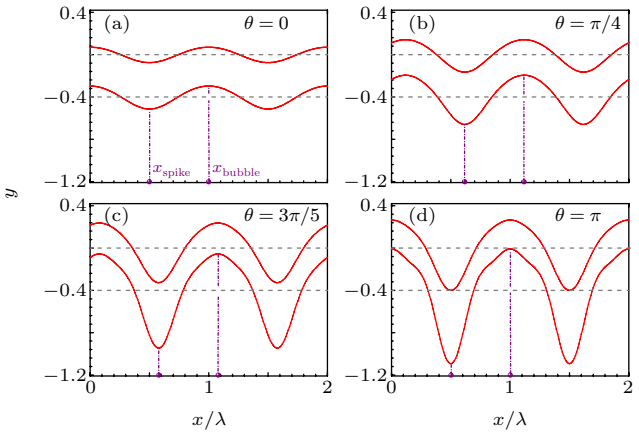


Fig. 2. Temporal evolutions of interface positions of upper and lower interfaces at $\gamma t = 5.0$ for phase difference $\theta = 0$ (a), $\pi/4$ (b), $3\pi/5$ (c), and π (d). The dashed lines represent the unperturbed shell with shell thickness $kd = 0.4$. The initial perturbations are $A_0 = B_0 = 0.001\lambda$.

The distance between the adjacent bubble and the spike is $\lambda/2$, which implies that the main structure of the interface caused by RTI for different θ remains unchanged (retaining the characteristics of single-mode RTI perturbation). However, the positions of the bubble and the spike are related to θ. The position of the spike corresponds to the position where the perturbation amplitude is maximum, which can be obtained using the formulas (16), (18), and (19), as

$$\tan(kx_{\rm spike}) = \frac{\sin\theta}{(A_0/B_0)e^{\xi} - \cos\theta}, \tag{27}$$

the explicit dependence of thickness ξ and phase difference θ are shown. The dependences of the spike position $x_{\rm spike}$ on kd and θ are displayed in Fig. 3. As the phase difference θ increases to π, the normalized spike position $x_{\rm spike}/\lambda$ increases gradually to the maximum and then decreases to 0.5. The larger shell thickness kd results in the smaller the maximum position of the spike under the same conditions. When kd approaches 4.0, the position of the spike is not affected by the phase difference, as the upper and lower interfaces are decoupled for a thick shell. We can also obtain from Eq. (27) that the position of the spike is determined by the coupling between two interfaces in the linear stage. The specific shape and growth of bubble–spike asymmetry are also affected by the phase difference which will be discussed later. Thus, it is found that phase difference of perturbations on two interfaces play an important role in the WN evolution of the shell, especially for $kd < 1$. In typical ICF implosions, a thin shell is imploded inward, phase difference will cause the spike of the fluid to move in the vertical direction of the implosion acceleration. Then, the integrity of the shell will be destroyed, which will accelerate the mixing of ablated materials and DT fuel, thereby affect implosion compression and reduce energy gain.

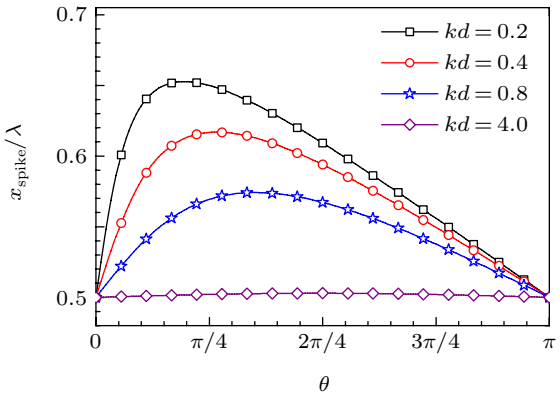


Fig. 3. The position of the spike tip $x_{\rm spike}/\lambda$ *versus* the initial phase difference θ for $kd = 0.2$, 0.4, 0.8, and 4.0. The initial perturbations are $A_0 = B_0 = 0.001\lambda$.

The distortion of the shell is exhibited in Fig. 4 by studying the evolution of shell thickness $d_{\rm spike}$ at the spike tip and $d_{\rm bubble}$ at the bubble vertex. The evolution of normalized $d_{\rm spike}/d$ and $d_{\rm bubble}/d$ with different θ are displayed in this figure. The shell thickness $d_{\rm spike}$ increases with time proceeding but $d_{\rm bubble}$ decreases with time γt. That means the growth of

finite-thickness RTI exacerbates the deformation of the shell. As can be seen, the $d_{\rm spike}$ increases with θ but $d_{\rm bubble}$ decreases with θ. Thus, the in phase case ($\theta = 0$) for the growth of perturbation at the two interfaces of the shell will underestimate the perturbation growth. The phase difference of perturbation should be considered when predicting shell deformation in ICF implosions.

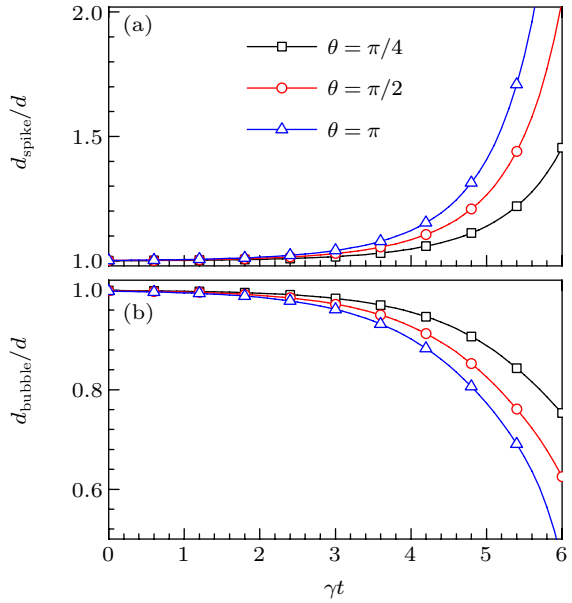


Fig. 4. Temporal evolutions of shell thickness at the spike tip (a) and the bubble vertex (b) for initial shell thickness $kd = 0.5$. The initial phase differences are $\theta = \pi/4$, $\pi/2$, and π, respectively.

In Fig. 5, the evolution of dimensionless velocity $v_{\rm spike}(k/g)^{1/2}$ of spike and $v_{\rm bubble}(k/g)^{1/2}$ of bubble for different initial phase difference θ are analyzed. The velocity of spike tip $v_{\rm spike}$ increases with time, the larger phase difference θ leads to larger spike velocity. The velocity of bubble vertex $v_{\rm bubble}$ grows gradually with time, the bubble velocity is sightly affected by phase difference θ. The velocity of spike is sensitivity to the phase difference until late nonlinear stage. Therefore, it is necessary to consider the influence of the initial phase difference on the perturbation growth in ICF implosion.

Temporal evolutions of fundamental mode $\eta^{(1)}_{\rm cos}/\lambda$ for cosine mode perturbation are displayed in Fig. 6(a) and the corresponding second harmonic generation $-\eta^{(2)}_{\rm cos}/\lambda$ is shown in Fig. 6(b). For different phase difference θ, the $\eta^{(1)}_{\rm cos}$ grows gradually to a maximum with time γt, and then decreases quickly. Since the decreasing amplitude in the WN stage is unrealistic, the scope of application of the third-order WN theory is before the fundamental mode exceeding the maximum amplitude. The large phase difference θ results in larger perturbation growth of the fundamental mode. The negative amplitude $-\eta^{(2)}_{\rm cos}$ means the phase of the second harmonic changes by π in comparison to the fundamental mode. When the second harmonic is generated, the bubble-spike structure on the interface is formed. As can be seen, the larger θ leads to larger perturbation amplitude $-\eta^{(2)}_{\rm cos}$, the more round bubble tip and more narrow spike tip can be obtained. Thus, we can conclude that the perturbation growth and bubble–spike deformation are affected by θ, which is consistent with the phenomenon observed in Fig. 2.

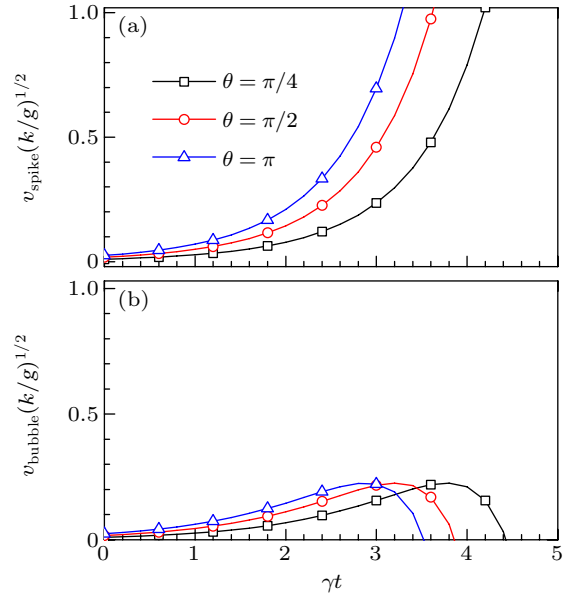


Fig. 5. Temporal evolutions of the velocity of spike tip $v_{\rm spike}(k/g)^{1/2}$ (a) and bubble vertex $v_{\rm bubble}(k/g)^{1/2}$ (b) at the lower interface of the shell. The initial phase differences are $\theta = \pi/4$, $\pi/2$, and π, respectively.

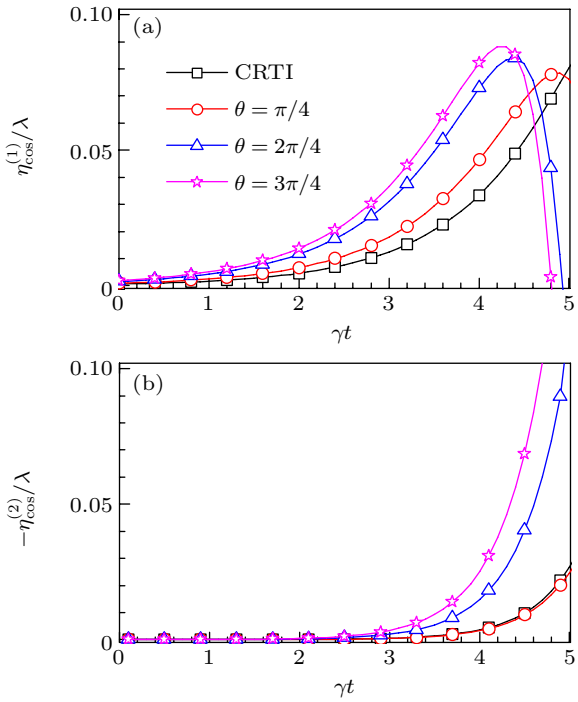


Fig. 6. Temporal evolution of normalized amplitudes of the perturbation fundamental mode $\eta^{(1)}_{\rm cos}/\lambda$ (a) and the second harmonic $-\eta^{(2)}_{\rm cos}/\lambda$ (b). The initial phase differences are $\theta = 0$ (CRTI), $\pi/4$, $\pi/2$, and $3\pi/5$, respectively.

Temporal evolutions of the fundamental mode $\eta^{(1)}_{\rm sin}/\lambda$ and the second harmonic $-\eta^{(2)}_{\rm sin}/\lambda$ for sine mode perturbation are displayed in Figs. 7(a) and 7(b), respectively. When the perturbations on the upper and lower interfaces are initiated with an arbitrary phase difference θ, the sine-mode perturbation will

be generated. The interaction of the cosine mode and the sine mode causes the positions of the bubble and the spike to be related to the initial phase difference θ. When $\gamma t = 4.0$ and $kd = 0.5$, the sine-mode perturbation $\eta^{(1)}_{\sin}/\lambda$ is ~ 0.035, 0.044 and 0.04 for $\theta = \pi/4$, $2\pi/4$, and $3\pi/5$. Thus, the different θ leads to different growth of the sine mode, which causes the positions of bubbles and spikes to rely on θ. The second harmonic $-\eta^{(2)}_{\sin}/\lambda$ also plays an important role in the development of bubble-spike structure. The amplitude of the second harmonic depends on shell thickness d and phase difference θ. For $kd = 0.5$, the amplitude $-\eta^{(2)}_{\sin}$ is approximately related to $\sim \sin\theta$, so the perturbation amplitudes are approximately the same for $\theta = \pi/2$ and $3\pi/5$,which can be seen in Fig. 7(b). The sine-mode perturbations are disappeared for $\theta = 0$ which means the results for previous finite-thickness RTI growth are recovered.[23,24]

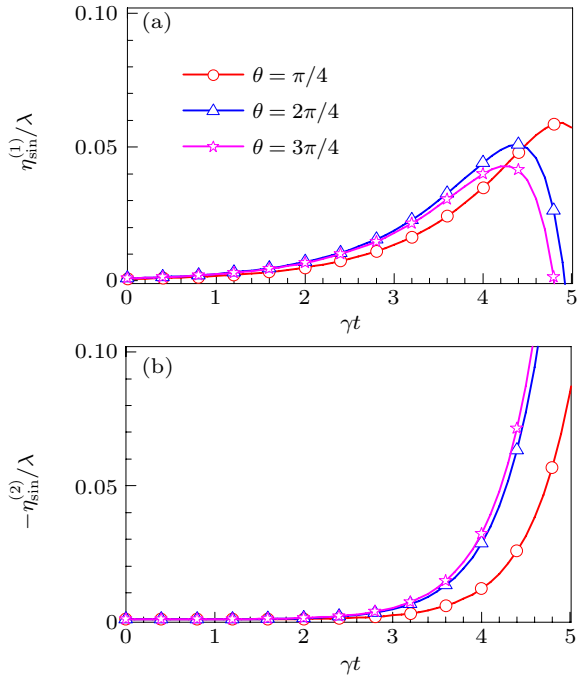


Fig. 7. Temporal evolutions of normalized amplitudes of the perturbation fundamental mode $\eta^{(1)}_{\sin}/\lambda$ (a) and the second harmonic $-\eta^{(2)}_{\sin}/\lambda$ (b). The initial phase differences are $\theta = \pi/4$, $\pi/2$, and $3\pi/5$, respectively.

4. Conclusion

The WN model for RTI growth of finite-thickness incompressible shell is investigated analytically, considering that there is an arbitrary phase difference for the perturbations at the upper and lower interfaces. The third-order solutions are obtained to describe the perturbation growth and the shell deformation. When the phase difference $\theta = 0$, the WN results for RTI growth of a finite-thickness slab are recovered.[24] The phase difference plays an important role in perturbation growth and the deformation of imploded shell for ICF implosions. The larger θ leads to more obvious bubble-spike structures at the shell interfaces. That means larger θ results in more round bubble shape and more narrow spike tip. Meanwhile, the positions of bubble and spike are dependent on shell thickness d and phase difference θ. For a thin shell implosion, the initial cosine-mode perturbations on two interfaces are coupled, and the sine-mode perturbation will be generated with the time proceeding which affects the position of bubble-spike structure. The analytical model is expected to improve the understanding of the interface coupling and initial perturbation phase effect on the RTI growth of a finite-thickness shell in ICF implosion. It is notable that the potential influences of compressibility are not included in our model. They are quite important for ICF. Considerations of compressibility effects are beyond the scope of this work, which will be pursued in the future.

Acknowledgments

Project supported by the Fundamental Research Funds for the Central Universities, China (Grant No. 2021YQLX05), the National Natural Science Foundation of China (Grant No. 11974419), and the Strategic Priority Research Program of the Chinese Academy of Sciences (Grant Nos. XDA 25051000).

References

[1] Rayleigh L 1883 *Proc. London Math. Soc.* **14** 170
[2] Taylor G 1950 *Proc. R. Soc. Lond. A* **201** 192
[3] Chittenden J P and Jennings C A 2008 *Phys. Rev. Lett.* **101** 055005
[4] Lindl J D, Amendt P, Berger R L, Glendinning S G, Glenzer S H, Haan S W, Kauffman R L, Landen O L and Suter L J 2004 *Phys. Plasmas* **11** 339
[5] Wang L F, Ye W H, He X T, Wu J F, Fan Z F, Xue C, Guo H Y, Miao W Y, Yuan Y T, Dong J Q, Jia G, Zhang J, Li Y J, Liu J, Wang M, Ding Y K and Zhang W Y 2017 *Sci. China-Phys. Mech. Astron.* **60** 055201
[6] Jacobs J W and Catton I 1988 *J. Fluid Mech.* **187** 329
[7] Liu W H, Wang L F, Ye W H and He X T 2012 *Phys. Plasmas* **19** 042705
[8] Wang L F, Wu J F, Fan Z F, *et al.* 2012 *Phys. Plasmas* **19** 112706
[9] Lai H L, Xu A G, Zhang G C, *et al.* 2016 *Phys. Rev. E* **94** 023106
[10] Zhang J, Wang L F, Ye W H, Wu J F, Guo H Y, Zhang W Y and He X T 2017 *Phys. Plasmas* **24** 062703
[11] Xin J, Yan R, Wan Z H, Sun J, Zheng J, Zhang H, Aluie H and Betti R 2019 *Phys. Plasmas* **26** 032703
[12] Mikaelian K O 1982 *Phys. Rev. A* **26** 2140
[13] Mikaelian K O 1983 *Phys. Rev. A* **28** 1637
[14] Guo H Y, Wang L F, Ye W H, *et al.* 2017 *Chin. Phys. Lett.* **34** 075201
[15] Guo H Y, Wang L F, Ye W H, *et al.* 2017 *Chin. Phys. B* **26** 125202
[16] Guo H Y, Wang L F, Ye W H, *et al.* 2018 *Chin. Phys. B* **27** 025206
[17] Weis M R, Zhang P, Lau Y Y, *et al.* 2014 *Phys. Plasmas* **21** 122708
[18] Velikovich A L and Schmit P F 2015 *Phys. Plasmas* **22** 122711
[19] Plesset M S 1954 *J. Appl. Phys.* **25** 96
[20] Wilkinson J P and Jacobs J W 2007 *Phys. Fluids* **19** 124102
[21] Jacobs J W and Catton I 1988 *J. Fluid Mech.* **187** 353
[22] Ding J C, Si T, Yang J M, *et al.* 2017 *Phys. Rev. Lett.* **119** 014501
[23] Wang L F, Guo H Y, Wu J F, *et al.* 2014 *Phys. Plasmas* **21** 122710
[24] Guo H Y, Wang L F, Ye W H, *et al.* 2017 *Phys. Plasmas* **24** 112708
[25] Miles A R, Edwards M J, Blue B, *et al.* 2004 *Phys. Plasmas* **11** 5507